Mechanical Systems and Signal Processing 120 (2019) 793–807

Contents lists available at ScienceDirect

Mechanical Systems and Signal Processing

journal homepage: www.elsevier.com/locate/ymssp

A method for numerical and experimental nonlinear modal analysis of nonsmooth systems

Simon Peter *, Frederic Schreyer, Remco I. Leine

Institute for Nonlinear Mechanics, University of Stuttgart, Pfaffenwaldring 9, 70569 Stuttgart, Germany

ARTICLE INFO

Article history:
Received 15 June 2018
Received in revised form 10 September 2018
Accepted 7 November 2018

Keywords:
Nonlinear modes
Nonsmooth systems
Nonlinear modal analysis
Mixed Shooting-Harmonic Balance Method
Nonlinear phase resonance testing

ABSTRACT

The development of nonlinear modal analysis so far has focused on structures with smooth nonlinearities. However, nonsmooth nonlinearities, which are, for instance, caused by contact interactions are highly relevant in practical applications. This paper proposes a novel numerical approach along with a method for the measurement of nonlinear modes of structures with nonsmooth contact nonlinearities.

The proposed numerical method combines the shooting method and the harmonic balance method, yielding a mixed time-frequency domain representation of the system, allowing for an efficient treatment of the nonsmooth contact law within the numerical approach. Moreover, the mass of the system is redistributed such that the contact nodes are massless. Thereby, the dynamic contact problem can be reduced to a quasi-static contact problem. A salient feature of this numerical approach is that the contact problems are solved without the need for any contact parameters, such as penalty or restitution coefficients. Furthermore, the conservative nature of the contact law incorporated in this formulation allows for the calculation of nonlinear modes as periodic solutions of conservative systems.

The experimental method relies on a nonlinear phase resonance approach. Hitherto, phase resonance methods have exclusively been applied to systems with smooth nonlinearities. In this study, an automated nonlinear phase resonance approach with phase-controlled excitation is used, providing a robust experimental procedure, which facilitates the treatment of strong nonsmooth nonlinearities, e.g., caused by unilateral constraints inducing impacts.

The numerical and experimental methods are demonstrated by an application to a benchmark structure consisting of a beam with one-sided support leading to impacts. It is shown that the numerical method can be applied without the need for any nonlinear system identification effort and the results agree well with the measured nonlinear modes.

1. Introduction

Modal analysis is by far the most widely used method for the experimental and numerical investigation of linear dynamic structures. However, the increasing complexity of engineering structures and the demand for cost-efficient designs often reveals the boundaries of linear models. Nonlinearity can even open a new design space, which allows for superior dynamic

* Corresponding author.
E-mail addresses: peter@inm.uni-stuttgart.de (S. Peter), schreyer@inm.uni-stuttgart.de (F. Schreyer), leine@inm.uni-stuttgart.de (R.I. Leine).

https://doi.org/10.1016/j.ymssp.2018.11.009
0888-3270/

performance compared to linear designs. For instance, nonlinear damping effects in frictional contacts of bladed disks are exploited in aircraft engines [1]. Another example, where nonlinear effects are deliberately introduced to a structure, is the design of nonlinear vibration absorbers using nonlinear targeted energy transfer [2]. These examples highlight the need for experimental and numerical methods for the treatment of nonlinear structures. In fact, in the former example it is obvious that nonsmooth effects, such as friction in contact interfaces, are of particular relevance. Regarding the latter, it is shown in several studies that nonsmooth effects, i.e., impacts, can be beneficial if very fast energy transfer is desired [3,4].

The design of nonlinear vibration absorbers is often based on the concept of nonlinear modes, which was originally proposed by Rosenberg [5]. Nonlinear modes, defined as periodic solutions of an autonomous conservative system, are the subject of numerous publications [6–8]. However, most numerical [9,10] and experimental studies [11–13] on nonlinear modal analysis focus on smooth nonlinearities. It is not clear to which extent the used methods can be applied to systems with nonsmooth nonlinearities and how this could be accomplished. Therefore, this paper proposes strategies for numerical and experimental modal analysis which are particularly suitable for the investigation of structures with nonsmooth nonlinearities.

Most work in the field of numerical nonlinear modal analysis of nonsmooth structures is limited to systems of low complexity [14] or based on regularization of nonsmooth contact laws [15,16]. Nonsmooth effects are described by set-valued force laws, i.e., Signorini's law, inequality complementary impact laws and friction laws, which lead to measure differential inclusions that require specific numerical solution techniques such as time-stepping methods [17]. Moreover, the strongly nonlinear effects induced by nonsmooth nonlinearities such as unilateral constraints inducing impacts lead to complex nonlinear modal dynamics even for comparatively simple structures [18], which makes the extension to large scale systems difficult. Regularized contact models, which replace the set-valuedness by a single-valued function, allow for the calculation of nonlinear modes with standard methods such as harmonic balance methods (HBM). A particular advantage of HBM approaches is that the choice of ansatz functions allows for the filtering of internal resonances [19] which reduces the complexity of the nonlinear modal dynamics and, thereby, the computational burden. However, the required regularization often leads to unphysical contact behavior, e.g., penetration of the contact surfaces, and involves the choice of artificial contact stiffness [20] or penalty parameters [21]. In this paper, a novel numerical method for the calculation of nonlinear modes is proposed, which is based on a mixed time-frequency domain formulation. The method is an extension of the Mixed Shooting-HBM (MS-HBM) with redistributed mass matrix [22] to nonlinear mode calculation. It will be shown that this method is particularly suitable for nonlinear modal analysis of unilaterally constrained systems, as it combines the filtering property with the possibility of including set-valued force laws. Moreover, the method does not require any contact parameter and is energy consistent, such that the system is conservative and its nonlinear modes can be defined as periodic solutions.

In the field of nonlinear experimental modal analysis (NEMA) most research is conceptually based on the pioneering work of Peeters [12] who proposed an extension of the phase resonance method to nonlinear systems. The practical realization, as a combination of a manually appropriated force with a time-frequency analysis of the free-decay, has been applied to several test structures [13,23,24]. Practical deficiencies of the method motivated the development of automated phase resonance techniques in the framework of control based continuation [25] and with phase control strategies [11,26]. All of these studies have in common that they exclusively cover structures with smooth nonlinearities. A completely different approach for nonlinear modal based system identification, which relies on signal processing techniques, is the so-called empirical mode decomposition [27]. This method has successfully been applied to nonsmooth mechanical systems [28,29]. However, the drawback of the method compared to nonlinear phase resonance approaches is that the obtained intrinsic modal oscillators lack a clear physical meaning.

To overcome the limitations of the previous experimental approaches, the present paper explores the capability of nonlinear phase resonance testing to treat structures with strong nonsmooth nonlinearities. To this end, the Phase-Locked-Loop (PLL) based phase resonance testing procedure proposed in [30] is applied to a structure with unilateral constraints inducing impacts. It will be shown that the method is robust for such strongly nonlinear systems and that a phase controlled single point excitation can be sufficient to isolate a nonlinear mode to a satisfying accuracy.

The paper is organized as follows. The theoretical background of the numerical and the experimental method is outlined in Section 2. A numerical example in Section 3 illustrates the properties of the numerical method. Both, the numerical and experimental method, are applied to a benchmark structure which is described in Section 4. The results are presented and discussed in Section 5. The paper closes with a conclusion and indicates directions of future work in Section 6.

2. Theoretical background

This section clarifies the definition of nonlinear modes used in this paper and covers the necessary theory of the proposed numerical as well as the experimental method.

2.1. Nonlinear modes

For the definition of modes of linear structures, there is more or less consensus in literature. For nonlinear structures, however, there exist different concurrent definitions of a nonlinear mode such that the definition used in this paper needs to be clarified. The two fundamental definitions can be traced back to the work of Rosenberg [5] and Shaw and Pierre [31].

The definition used in this paper is essentially based on Rosenberg's definition, which evolved over the years to include the phenomenon of internal resonance [6]. Thus, a nonlinear mode is defined as periodic solution $\mathbf{q}_{\mathrm{nm}}(t) = \mathbf{q}_{\mathrm{nm}}\left(t + \widetilde{T}_0\right)$ with the period time $\widetilde{T}_0$ of an autonomous, conservative, nonlinear system in a spatially discretized form

$$\mathbf{M}\ddot{\mathbf{q}}(t) + \mathbf{K}\mathbf{q}(t) + \mathbf{f}_{\mathrm{nl}}(\mathbf{q}(t)) = \mathbf{0}, \tag{1}$$

where $\mathbf{M} = \mathbf{M}^{\mathrm{T}} \in \mathbb{R}^{m\times m}$ denotes the positive definite mass matrix, $\mathbf{K} = \mathbf{K}^{\mathrm{T}} \in \mathbb{R}^{m\times m}$ the positive definite linear stiffness matrix, $\mathbf{q}(t) \in \mathbb{R}^m$ represents the vector of generalized coordinates and $\mathbf{f}_{\mathrm{nl}}(\mathbf{q}(t)) \in \mathbb{R}^m$ represents the vector of nonlinear conservative forces.

The motivation for the use of Rosenberg's definition is twofold: firstly, the numerical calculation of nonlinear modes as periodic solutions of the underlying conservative system is comparatively straightforward and, secondly, the experimental methods which have so far been proposed also mostly rely on Rosenberg's definition. Regarding the former, it is noted that, particularly for nonsmooth systems, the occurrence of internal resonances is highly probable. Therefore, the parameterization of an invariant manifold according to the definition of Shaw and Pierre [31] would generally be difficult. Furthermore, in this study, the focus is put on unilaterally constrained systems subjected to impacts. The numerical modeling of the highly complex damping mechanisms due to impacts is associated to several difficulties, which is discussed in some detail in Section 5.1. Regarding the experimental methods, the direct measurement of an invariant manifold of the damped free system seems to be very difficult as the realization of an initial condition on the invariant manifold without an a priori knowledge of its shape is infeasible.

2.2. Numerical method: Mixed Shooting-Harmonic Balance with redistributed mass matrix

Several numerical methods exist to calculate the periodic solutions of the autonomous system, mathematically described through (1). The shooting method [9] and the HBM [10] are the most well established approaches. In case the nonlinear force stems from one-sided supports (i.e. a contact) either hard or compliant, the nonlinear force can generally be expressed as

$$\mathbf{f}_{\mathrm{nl}} = -\sum_{i=1}^{c} \mathbf{w}_i \lambda_i = -\mathbf{W}\boldsymbol{\lambda}, \tag{2}$$

where $\mathbf{w}_i$ is the generalized force direction of the ith contact force λ_i. Often, the contact is modeled using a penalty approach, where

$$-\lambda_i = \begin{cases} k_{\mathrm{c}} g_i & \text{if} \quad g_i = \mathbf{w}_i^{\mathrm{T}}\mathbf{q} + g_{0,i} < 0 \\ 0 & \text{if} \quad g_i \geqslant 0 \end{cases} \tag{3}$$

is simply described as a function of $\mathbf{q}$ using an unphysical contact stiffness $k_{\mathrm{c}} > 0$ to penalize the penetration derived from the gap function g_i. Herein, g_i is assumed to be an affine function in $\mathbf{q}$ for simplicity, where $g_{0,i}$ is the offset.

In the present paper, the contact is modeled as a hard unilateral constraint and therefore it is necessary that the numerical solver can handle set-valued force laws within the nonlinear mode calculation. Hence, the finite element system

$$\mathbf{M}\ddot{\mathbf{q}}(t) + \mathbf{K}\mathbf{q}(t) = \mathbf{W}\boldsymbol{\lambda}(t), \tag{4}$$

with the inequality complementarity condition

$$0 \leqslant \mathbf{g}(t) \perp \boldsymbol{\lambda}(t) \geqslant 0, \quad \mathbf{g}(t) = \mathbf{W}^{\mathrm{T}}\mathbf{q}(t) + \mathbf{g}_0 \tag{5}$$

has to be solved which forces the system to satisfy the non-penetration condition exactly. To solve the system in time domain through numerical integration, generally, the differential Eq. (4) is complemented with an impact equation and an impact law with restitution coefficient is introduced. The equations are then solved using Moreau's time stepping scheme [17]. Hence, the shooting method can still be used to calculate nonlinear modes. But for large scale systems with many degrees of freedom DOFs the shooting method becomes infeasible. Moreover, the concept of nonlinear modes defined as periodic motions of the underlying conservative system excludes dissipative mechanisms such that in this framework only a coefficient of restitution of $e_{\mathrm{N}} = 1$ is admissible. Even worse, it has been observed in a previous study that a coefficient of $e_{\mathrm{N}} = 1$ leads to spurious high frequency vibrations when used in a finite element model and that the impact process can be accurately represented by the internal waves propagating in the finite element structure [32]. In contrast to the shooting approach, the global harmonic ansatz functions used within the HBM framework are efficient for large systems but are unable to fulfill the non-penetration condition directly. Due to the numerical issues related to the shooting method and the unsuitable ansatz functions of HBM, in this paper the MS-HBM with redistributed mass matrix [32] is introduced to numerically obtain the nonlinear modes of the unilaterally constrained system in Eq. (4).

In many finite element systems only a few DOFs are part of the contact area and therefore are directly subjected to set-valued forces. The MS-HBM exploits this local character of the nonlinearities to solve unilaterally constrained systems efficiently. Dividing the system's DOFs into linear DOFs, i.e., DOFs at which no nonlinear forces act, with the associated generalized coordinates $\mathbf{q}_{\mathrm{L}}$ and nonlinear DOFs, i.e., DOFs at which nonlinear forces act, with the associated generalized coordinates $\mathbf{q}_{\mathrm{N}}$ yields

$$\begin{pmatrix} \mathbf{M}_{\mathrm{LL}} & \mathbf{M}_{\mathrm{LN}} \\ \mathbf{M}_{\mathrm{NL}} & \mathbf{M}_{\mathrm{NN}} \end{pmatrix} \begin{pmatrix} \ddot{\mathbf{q}}_{\mathrm{L}} \\ \ddot{\mathbf{q}}_{\mathrm{N}} \end{pmatrix} + \begin{pmatrix} \mathbf{K}_{\mathrm{LL}} & \mathbf{K}_{\mathrm{LN}} \\ \mathbf{K}_{\mathrm{NL}} & \mathbf{K}_{\mathrm{NN}} \end{pmatrix} \begin{pmatrix} \mathbf{q}_{\mathrm{L}} \\ \mathbf{q}_{\mathrm{N}} \end{pmatrix} = \begin{pmatrix} \mathbf{0} \\ \bar{\mathbf{W}}\boldsymbol{\lambda} \end{pmatrix}, \tag{6}$$

where the nonlinear forces only depend and act on the nonlinear subsystem. The main idea of MS-HBM is to describe the linear subsystem in frequency domain and the nonlinear subsystem in time domain. This approach allows that only the linear subsystem is harmonically constrained and hence the non-penetration condition can be considered within the nonlinear subsystem.

The linear subsystem is constrained to the multi-harmonic oscillation

$$\mathbf{q}_{\mathrm{L}}(t) = \mathrm{Re}\left\{ \sum_{n=0}^{N_h} \underline{\mathbf{q}}_{\mathrm{L},n} \exp^{\mathrm{i}n\omega t} \right\}, \tag{7}$$

described by a Fourier series with the complex Fourier coefficients $\underline{\mathbf{q}}_{\mathrm{L},n}$, which is truncated to a finite number of harmonics N_h for practical reasons. Since all higher harmonic force components which are not included in the ansatz functions are counterbalanced by the multi-harmonic constraint, the linear subsystem can be described in frequency domain

$$\mathbf{H}_{\mathrm{LL}}\underline{\mathbf{q}}_{\mathrm{L}} + \mathbf{H}_{\mathrm{LN}}\underline{\mathbf{q}}_{\mathrm{N}} = \mathbf{0} \quad \text{with} \quad \underline{\mathbf{q}}_{\mathrm{L}} = \left[\underline{\mathbf{q}}_{\mathrm{L},0}^{\mathrm{T}}, \ldots, \underline{\mathbf{q}}_{\mathrm{L},N_h}^{\mathrm{T}} \right]^{\mathrm{T}} \tag{8}$$

and the vector $\underline{\mathbf{q}}_{\mathrm{N}}$ containing the complex Fourier coefficients of the nonlinear subsystem. Herein, the dynamic stiffness matrices are defined as

$$\mathbf{H}_{\mathrm{ij}} = \mathrm{diag}\left(\mathbf{H}_{\mathrm{ij},0}, \mathbf{H}_{\mathrm{ij},1}, \ldots, \mathbf{H}_{\mathrm{ij},N_h}\right) \quad \text{with} \quad \mathbf{H}_{\mathrm{ij},n} = -\mathbf{M}_{\mathrm{ij}}(n\omega)^2 + \mathbf{K}_{\mathrm{ij}}, \tag{9}$$

where the subscripts $i,j \in \{\mathrm{L},\mathrm{N}\}$ indicate the subsystem and $n \in \mathbb{N}_0^+$ the harmonic number.

The nonlinear subsystem

$$\mathbf{M}_{\mathrm{NN}}\ddot{\mathbf{q}}_{\mathrm{N}} + \mathbf{K}_{\mathrm{NN}}\mathbf{q}_{\mathrm{N}} + \mathbf{M}_{\mathrm{NL}}\ddot{\mathbf{q}}_{\mathrm{L}} + \mathbf{K}_{\mathrm{NL}}\mathbf{q}_{\mathrm{L}} = \bar{\mathbf{W}}\boldsymbol{\lambda} \tag{10}$$

$$0 \leqslant \mathbf{g}(t) \perp \boldsymbol{\lambda}(t) \geqslant 0, \quad \mathbf{g}(t) = \bar{\mathbf{W}}^{\mathrm{T}}\mathbf{q}(t) + \mathbf{g}_0 \tag{11}$$

remains in time domain to allow for the fulfillment of the non-penetration condition. Instead of using a restitution coefficient, Khenous shows in [33] that for fine discretized finite element systems it is reasonable to use a massless boundary approach to solve unilaterally constrained systems of finite element models. Hereto, the mass matrix is redistributed in such a way that the contact area becomes massless. Generally, the redistribution of the mass matrix of a finite element model affects the dynamic behavior of the model, e.g., the eigenfrequencies and mode shapes. However, the effect of the redistribution on the global dynamic behavior can be minimized by using a locally refined mesh of the finite element model near the contact area. Moreover, an optimization procedure can be used to retain characteristic features of the model such as the total mass, center of gravity or moment of inertia. For a more detailed discussion the reader is referred to [32,33]. In the present paper, where academic examples are used to demonstrate the method, the mass of the contact node is simply neglected. This approach leads to a small change in eigenfrequencies and mode shapes compared to the original model. In the experimental demonstration in Section 4 this error is minimized by directly updating the redistributed model to fit the experimental data obtained by a linear experimental modal analysis. The system with the redistributed mass matrix $\mathbf{M}_{\mathrm{R}}$ can therefore be rewritten as

$$\underbrace{\begin{pmatrix} \bar{\mathbf{M}}_{\mathrm{LL}} & \mathbf{0} \\ \mathbf{0} & \mathbf{0} \end{pmatrix}}_{\mathbf{M}_{\mathrm{R}}} \begin{pmatrix} \ddot{\mathbf{q}}_{\mathrm{L}} \\ \ddot{\mathbf{q}}_{\mathrm{N}} \end{pmatrix} + \begin{pmatrix} \mathbf{K}_{\mathrm{LL}} & \mathbf{K}_{\mathrm{LN}} \\ \mathbf{K}_{\mathrm{NL}} & \mathbf{K}_{\mathrm{NN}} \end{pmatrix} \begin{pmatrix} \mathbf{q}_{\mathrm{L}} \\ \mathbf{q}_{\mathrm{N}} \end{pmatrix} = \begin{pmatrix} \mathbf{0} \\ \bar{\mathbf{W}}\boldsymbol{\lambda} \end{pmatrix} \tag{12}$$

and the impact equation becomes superfluous. After splitting the redistributed system into the two coupled subsystems, the nonlinear subsystem

$$\mathbf{K}_{\mathrm{NN}}\mathbf{q}_{\mathrm{N}} + \mathbf{K}_{\mathrm{NL}}\mathbf{q}_{\mathrm{L}} = \bar{\mathbf{W}}\boldsymbol{\lambda} \tag{13}$$

simplifies to a static problem for which a linear complementarity problem (LCP) has to be solved for each time step. Hence, a nonlinear mode fulfills Eq. (13) together with Eq. (11) for each time step and the equation for the linear subsystem in Eq. (8). Furthermore, both subsystems are coupled through the connectivity condition

$$\underline{\mathbf{q}}_{\mathrm{N}} - \mathcal{F}(\mathbf{q}_{\mathrm{N}}(t)) = \mathbf{0} \tag{14}$$

given through the Fourier transformation $\mathcal{F}$.

To solve these equations a global LCP can be set up using the inverse Fourier transformation to substitute $\mathbf{q}_{\mathrm{L}}$ in Eq. (13) from Eq. (8). But since this LCP scales with the number of time steps multiplied by the number of nonlinear DOF, it is only reasonable for small systems. Therefore, an iterative solver is proposed to solve these equations efficiently.

The smallest possible vector of unknown

$$\mathbf{x} = \begin{pmatrix} \underline{\mathbf{q}}_{\mathrm{N}} \\ \omega \end{pmatrix} \tag{15}$$

with which the iteration process can be carried out, consist of the Fourier coefficients $\underline{\mathbf{q}}_{\mathrm{N}}$ of the nonlinear subsystem and the frequency of oscillation ω. The numerical scheme of the MS-HBM with redistributed mass matrix to calculate nonlinear modes with unilateral constraints is illustrated in Fig. 1. Using a prediction-correction path-following technique, the whole branch of a nonlinear mode is calculated starting from the linear eigenfrequency at a low energy level of the analyzed r-th mode. Therefore, the initial value of the unknowns $\mathbf{x}_0$ is extracted from the linear eigenvector $\boldsymbol{\phi}_r$ and the eigenfrequency $\omega_{0,r}$. The averaged kinetic energy over one period $E_{\mathrm{av}}\left(\omega, \underline{\mathbf{q}}_{\mathrm{N}}\right)$ serves as path-following parameter [34]. The description of the linear subsystem in frequency domain Eq. (8) yields, through the dynamic stiffness matrices, a linear relation between the Fourier coefficients of both subsystems. Therefore, the Fourier coefficients of the linear subsystem $\underline{\mathbf{q}}_{\mathrm{L}}$ can be directly calculated from $\underline{\mathbf{q}}_{\mathrm{N}}$ and a periodic motion can be fully described using the Fourier coefficients $\underline{\mathbf{q}}_{\mathrm{N}}$ of the nonlinear subsystem. Using an inverse Fourier transformation yields the time domain representation of $\underline{\mathbf{q}}_{\mathrm{L}}$ which is necessary to solve the LCP describing the nonlinear subsystem at each time step. Hereto, the inequality complementarity condition (11) is written as an implicit equation using a proximal point function [17].

A Newton-type predictor-corrector solver as proposed in [35] is used as path-following algorithm. Because the Fourier coefficients of the linear subsystem $\underline{\mathbf{q}}_{\mathrm{L}}$ can be directly calculated from $\underline{\mathbf{q}}_{\mathrm{N}}$, the size of the problem which needs to be solved iteratively is governed by the number of nonlinear DOFs, which is often small compared to the number of linear DOFs. A particular advantage of the MS-HBM with redistributed mass matrix is that the Jacobian matrix, which is required for the Newton-type method, can be calculated semi-analytically [32]. Therefore, the method is numerically efficient and also suitable for systems with many nonlinear DOFs. Since the absolute phase of the autonomous system is arbitrary, a phase anchor is used to obtain a unique solution. The phase anchor can simply be realized by setting one Fourier coefficient to zero. It is reasonable to choose a Fourier coefficient associated to the fundamental harmonic oscillation $\mathrm{Re}\left(\underline{q}_{\mathrm{a},1}\right) = 0$, such that the phase anchor is also suitable for purely fundamental harmonic oscillations. Finally, a residuum function for the Newton-type method has to be defined. The function

$$\mathbf{f}_{\mathrm{R}}(x) = \begin{pmatrix} \underline{\mathbf{q}}_{\mathrm{N}} - \mathcal{F}(\mathbf{q}_{\mathrm{N}}(t)) \\ E_{\mathrm{av}}\left(\omega, \underline{\mathbf{q}}_{\mathrm{N}}\right) - E_0 \end{pmatrix} \tag{16}$$

which has to be solved, consists of the connectivity condition which enforces the linear subsystem to oscillate in correspondence to the nonlinear subsystem and an energy condition which constrains the periodic solution to a specific energy level. Finally, after convergence is achieved, the parameters of the nonlinear mode are obtained in form of the modal frequency $\tilde{\omega}_{0,r}$ and the complex Fourier coefficients $\underline{\mathbf{q}}_{\mathrm{L}}$ and $\underline{\mathbf{q}}_{\mathrm{N}}$.

2.3. Experimental method: PLL based phase resonance testing

The experimental procedure followed in this work is conceptually based on the nonlinear phase resonance method which has originally been proposed by Peeters [12]. The fundamental idea is to balance out the damping forces by an appropriated

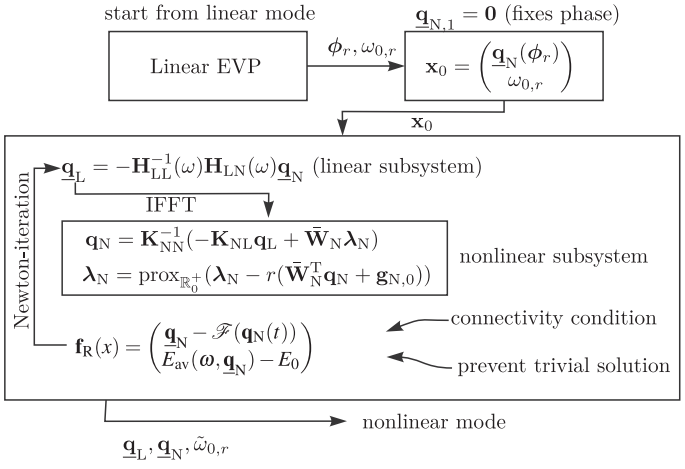

Fig. 1. Schematic numerical algorithm for the calculation of nonlinear modes using the MS-HBM.

excitation force such that the motion of the conservative autonomous system (cf. Eq. (4)) is imitated. It is shown in [12] for monophase motions and in [11] for more general cases based on power considerations that, in frequency domain, this excitation force has to be shifted in phase with respect to the displacement response by $\pi/2$ for all harmonics and all excitation points. For practical reasons, in most previous studies only the phase of the fundamental harmonic of a single point excitation force has been controlled either by manually adjusting the excitation frequency [12,23,36] or by automatic phase control using a PLL controller [30] or control based continuation [25].

For nonsmooth systems it is expected that the influence of high frequency vibrations increases compared to smooth nonlinear systems. Therefore, (a) the control of the phase and amplitude of the excitation force is more difficult and (b) the influence of higher harmonics at which no controlled excitation force is applied increases.

As a consequence of (a) the manual tuning of the excitation force, which is already difficult for smooth nonlinear systems [37], is infeasible such that a PLL based control strategy is pursued in the following. The PLL controller attached to a structure with shaker excitation is shown in a block diagram in Fig. 2 and only briefly described here. For a more comprehensive description, the reader is referred to [11,30]. The controller includes a phase detector block, of which the output is a function of the phase difference between the force and the displacement signal. The second part of the controller is the loop filter which suppresses oscillatory components of the phase detector output and minimizes the phase error using a proportional-integral (PI) controller. In the third part of the PLL the instantaneous phase for the voltage signal, which is used as an input of the shaker, is generated by a voltage controlled oscillator (VCO). This feedback loop can be interpreted as a means of generating an *autoresonant* system, as the instantaneous phase, i.e., also the forcing frequency, is a result of the system's response. This type of controller provides a high robustness for lightly damped and nonlinear systems as shown in [38] and proved to be applicable to a single DOF vibro-impact system [39]. The robustness of the method for continuous structures with nonsmooth nonlinearities is demonstrated in the following.

Considering (b), the stronger high frequency vibrations lead to stronger imperfections in the mode isolation compared to smooth systems. These imperfections can be quantified by relating the active power of the excitation [11]

$$P = \sum_{n=1}^{\infty} F_n V_n \cos(\varphi_n), \tag{17}$$

to the apparent power of the excitation

$$S = F_{\mathrm{RMS}} V_{\mathrm{RMS}} = \sqrt{\sum_{n=1}^{\infty} F_n^2} \sqrt{\sum_{n=1}^{\infty} V_n^2}. \tag{18}$$

Herein, F_n and V_n denote the effective values of the n-th harmonic of the force and the velocity, respectively, and φ_n the phase angle between force and velocity. The combination of both can be used as power based mode indicator function (PBMIF) defined as

$$\Lambda := -\frac{P}{S} \in [-1, 1], \tag{19}$$

which gives a value of unity in the case of a perfectly appropriated force [11].

2.4. Definition of nonlinear modal parameters

Once the nonlinear mode is appropriated to a satisfying accuracy, a nonlinear modal model can be extracted. The nonlinear modal model consists of an energy dependent nonlinear modal deflection shape and a nonlinear modal frequency. Furthermore, a modal damping measure can be extracted to capture the amplitude dependent damping characteristics. In the following the extraction of these modal parameters is briefly recapitulated. Particular emphasis is put on the consistency of

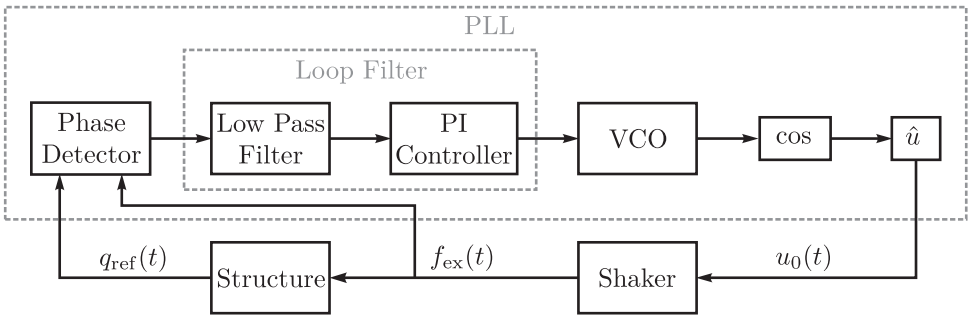

Fig. 2. Block diagram of PLL attached to a structure with shaker excitation.

the modal parameters with linear theory, which facilitates the interpretability of the modal parameters and is important for the use of the modal model for vibration prediction [37].

The *nonlinear modal frequency* $\tilde{\omega}_{0,r}$ of the r-th nonlinear mode can directly be obtained as an output of the PLL controller. The nonlinear mode shape can be obtained by Fourier transformation of the measured time signals. The nonlinear modal frequency is used to extract an integer multiple of the period length, such that leakage in the Fourier transform can be avoided. The nonlinear modal motion can then written as a Fourier series

$$\mathbf{q}_{\mathrm{nm},r}(t) = \mathrm{Re}\left\{\sum_{n=0}^{\infty} \underline{\tilde{\psi}}_{r,n} \exp^{\mathrm{i}n\tilde{\omega}_{0,r}t}\right\}, \tag{20}$$

in terms of an amplitude dependent mode shape $\underline{\tilde{\psi}}_{r,n}$ and the nonlinear modal frequency $\tilde{\omega}_{0,r}$. To ensure consistency to linear theory, where the mode shapes are most commonly normalized with respect to the mass matrix [40], Eq. (20) can be recast in the form [37]

$$\mathbf{q}_{\mathrm{nm},r}(t) = \mathrm{Re}\left\{\sum_{n=0}^{\infty} \tilde{q}_r \underline{\tilde{\phi}}_{r,n} \exp^{\mathrm{i}n\tilde{\omega}_{0,r}t}\right\}, \tag{21}$$

where $\tilde{q}_r$ denotes the *nonlinear modal amplitude* and $\underline{\tilde{\phi}}_{r,n}$ the *normalized nonlinear mode shape* of the r-th nonlinear mode. Herein, the mode shape is normalized such that the first harmonic of the nonlinear modal deflection shape is normalized with respect to the mass matrix, i.e.,

$$\underline{\tilde{\phi}}_{r,1}^{\mathrm{H}} \mathbf{M} \underline{\tilde{\phi}}_{r,1} = 1, \text{ with } \underline{\tilde{\phi}}_{r,n} = \frac{1}{\tilde{q}_r} \underline{\tilde{\psi}}_{r,n}. \tag{22}$$

Although the proposed nonlinear phase resonance approach aims at extracting the nonlinear modes of the underlying conservative system, it is possible to characterize the damping properties of the structure. Under the assumption of a conservative nonlinearity, the damping can be quantified based on the linearly damped and excited system

$$\mathbf{M}\ddot{\mathbf{q}}(t) + \mathbf{D}\dot{\mathbf{q}}(t) + \mathbf{K}\mathbf{q}(t) = \mathbf{f}_{\mathrm{ex}}(t) + \mathbf{W}\boldsymbol{\lambda}(t), \tag{23}$$

which represents the dissipative behavior of the experimental structure. In the case of a perfect mode isolation, the active power of the excitation force P is in balance with the mean dissipated power over one period [37], i.e.,

$$P = P_{\mathrm{diss}} = \frac{1}{T} \int_0^T \dot{\mathbf{q}}(t)^{\mathrm{T}} \mathbf{D} \dot{\mathbf{q}}(t) \mathrm{d}t, \tag{24}$$

where the dissipated power in the r-th mode can be written in terms of the above derived modal quantities in the frequency domain yielding

$$P_{\mathrm{diss}}^{r} = \sum_{n=1}^{\infty} \frac{1}{2} (n\tilde{\omega}_{0,r})^2 \tilde{q}_r^2 \underline{\tilde{\phi}}_{r,n}^{\mathrm{H}} \mathbf{D} \underline{\tilde{\phi}}_{r,n}. \tag{25}$$

In analogy to linear theory, a damping coefficient $\tilde{\delta}_{r,n}^{\mathrm{nl}}$ for the r-th nonlinear mode and the n-th harmonic can be defined as

$$\underline{\tilde{\phi}}_{r,n}^{\mathrm{H}} \mathbf{D} \underline{\tilde{\phi}}_{r,n} = 2\tilde{\omega}_{0,r} \tilde{\delta}_{r,n}^{\mathrm{nl}}. \tag{26}$$

This damping coefficient represents the damping behavior for each measured point on the nonlinear mode. Thereby, energy dependence of the damping, i.e., a deviation from the linear modal damping assumption, can be captured and quantified. Henceforth, the coefficient $\tilde{\delta}_{r,n}^{\mathrm{nl}}$ is referred to as *nonlinear modal damping* coefficient.

In first approximation the active power is mainly determined by its fundamental harmonic component such that the damping coefficient is approximated based on the fundamental harmonic power balance [37]

$$P_1 = P_{\mathrm{diss},1}^{r} = \tilde{\delta}_r^{\mathrm{nl}} \tilde{\omega}_{0,r}^3 \tilde{q}_r^2, \tag{27}$$

yielding

$$\tilde{\delta}_r^{\mathrm{nl}} = \frac{P_1}{\tilde{q}_r^2 \tilde{\omega}_{0,r}^3}, \tag{28}$$

which can then be used for amplitude dependent damping characterization.

3. Numerical example: Rod with unilateral constraint

The numerical method described in Chapter 2.2 is briefly illustrated by application to a unilaterally constrained rod. For the following numerical investigations, the parameters of the rod are given as the length $L = 20$ m, Young's modulus $E = 210 \cdot 10^9$ N/m^2 and its density $\rho = 9000$ kg/m^3. The finite element system describing the rod consists of 100 linear

elastic rod elements with a massless contact node at the tip. The initial size of the gap between the rod and the rigid ground is defined as $g_{N,0} = 0.5$ m. The nonlinear mode which is analyzed emerges from the first longitudinal linear mode of the system at 60.3 Hz. Fig. 3 (a) depicts an illustration of the considered system and Fig. 3 (b) shows the calculated frequency-energy plot. In the low energy regime, the nonlinear mode shape corresponds to the first linear eigenvector, scaled to the desired energy level. The nonlinear modal frequency does not change in the low energy regime, because the gap remains open for small motions. As soon as the rod oscillates with enough energy to hit the ground, the nonlinear modal frequency increases for all considered numbers of harmonics n_h. Generally, the calculated frequency-energy curves follow the same trend. However, if three or more harmonics are considered the branch changes significantly at a frequency of around 61 Hz. This region of the frequency-energy plot reveals the existence of an internal resonance, that has not been captured by the approximation with less than three harmonics. Indeed, the loop corresponds to a 3:1 internal resonance between the first and second longitudinal nonlinear mode, which has a linear eigenfrequency of around 182 Hz.

Taking a closer look at the mode shapes while following the loop, the energy transfer between the first and second modes becomes obvious. Fig. 4 visualizes the mode shapes at the points marked in Fig. 3 (a) on the branch. The blue line in Fig. 4

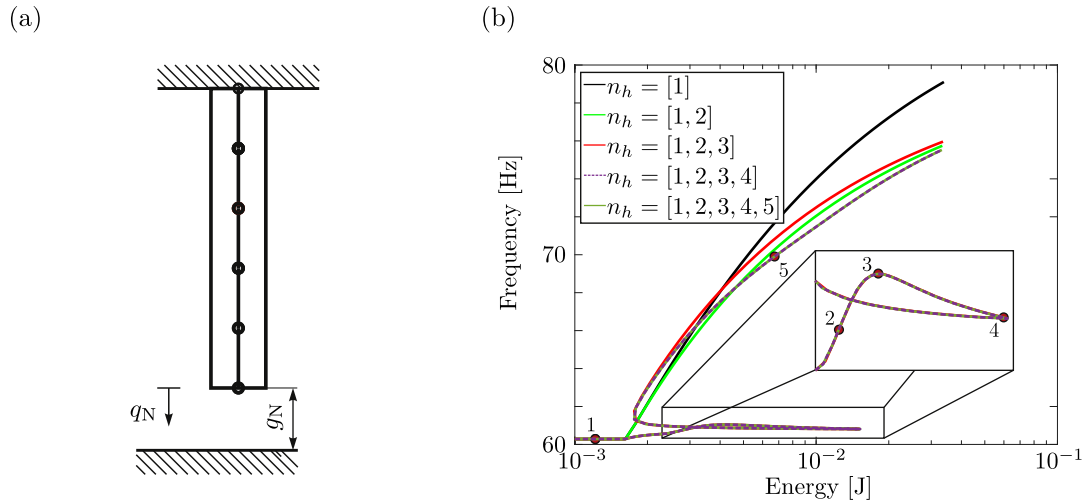

Fig. 3. Unilaterally constrained rod system (a) and its first nonlinear mode with different number of considered harmonics (b).

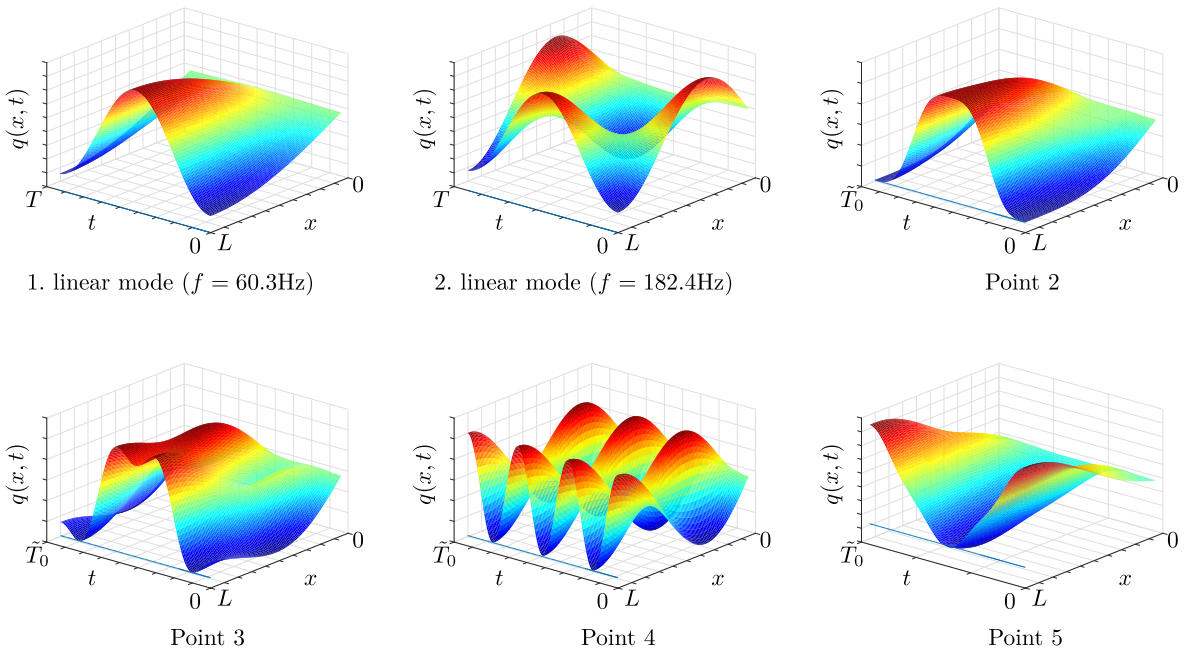

Fig. 4. Three dimensional illustration of the mode shapes of the rod in the 3:1 internal resonance.

represents the rigid ground. The 3*D* graph shows the oscillation q along the length L of the beam and the period time T. At the beginning of the loop the nonlinear mode is similar to the first linear mode shape (Point 1). Continuing along the branch to Points 2 and 3, respectively, more and more energy is transferred to the second mode. At the turning point (Point 4) the nonlinear mode shape corresponds exactly to the second linear mode shape and the frequency corresponds to the second modal frequency.

An interesting characteristic of the numerical method proposed here is that internal resonances can be analyzed, but similarly to conventional HBM approaches, the filtering property is retained. This filtering characteristic, which is not available in pure time domain methods such as the shooting method, can considerably save computational time. This is particularly interesting when the global behavior of the backbone curve of complex systems with many modal interactions is of interest, or in cases where modal interactions do not affect the behavior of the damped system. In the case of the present example, it can be seen that the approximation with two harmonics would be sufficient to capture the global dynamics of the system in the analyzed energy range but the 3:1 internal resonance is neglected. The example illustrates that already a small number of harmonics can be sufficient for the analysis of the global behavior of the backbone curve but a more detailed analysis of internal resonances can still be performed if this is desired. Thus, the computational effort of the proposed numerical approach can be adapted in a trade-off of accuracy and computation time.

4. Application to a benchmark beam structure

The proposed numerical and experimental approach is applied to a benchmark structure consisting of a beam with a one-sided support element, i.e., a stop. In this section, the experimental structure as well as the numerical model is described.

The experimental structure is shown in Fig. 5 and consists of a steel beam with rectangular cross section which is clamped at one end. The one-sided support is placed at the beam tip and consists of a load cell which is mounted onto a rigid steel block and equipped with a steel cap serving as contact surface. A magnification of the support element is also included in Fig. 5. The beam is excited with an electrodynamic shaker and the response is measured with six accelerometers and two laser doppler vibrometers (LDVs) with displacement decoders. The LDVs are placed at the excitation point and the beam tip. A schematic sketch of the setup is shown in Fig. 6. The PLL is implemented on a dSPACE DS1103 rapid prototyping system and all signals are recorded on two DeweBook DEWE-50-USB2-8 units at a sampling rate of 20 kHz. For the phase control, the measured excitation force and the displacement at the excitation point are used as reference signals. The displacement is used for the control rather than acceleration or velocity because it is less distorted by higher harmonics, increasing the robustness and accuracy of the control. The measured first six bending eigenfrequencies with the according modal damping values of the beam are shown in Table 1 (left). For the following nonlinear experimental modal analysis, the first bending mode is considered.

Two different numerical simulations are performed for comparison with the experimenetal results: a conventional HBM simulation with a contact stiffness model and the MS-HBM simulation as described above. The numerical model of the beam consists of 21 Timoshenko beam elements, i.e., 22 nodes with three DOFs each. The finite element discretization, which is indicated in Fig. 6, is refined towards the beam end. The refined mesh is used because in the numerical simulation with the MS-HBM the mass of the contact node is neglected. To obtain the unknown parameters of the numerical model, i.e.,

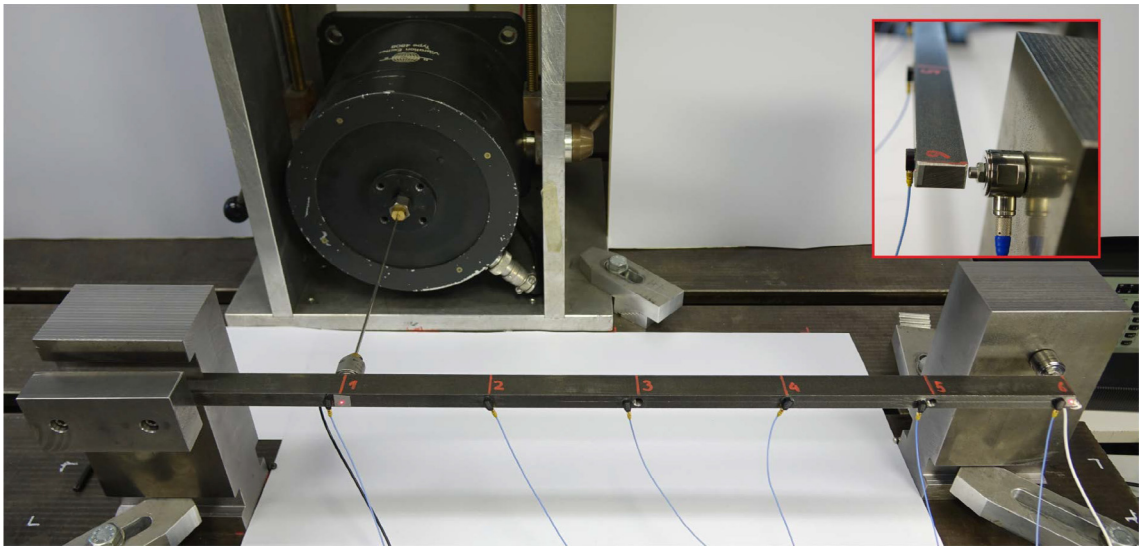

Fig. 5. Photo of the beam test rig with close-up of the one-sided support element.

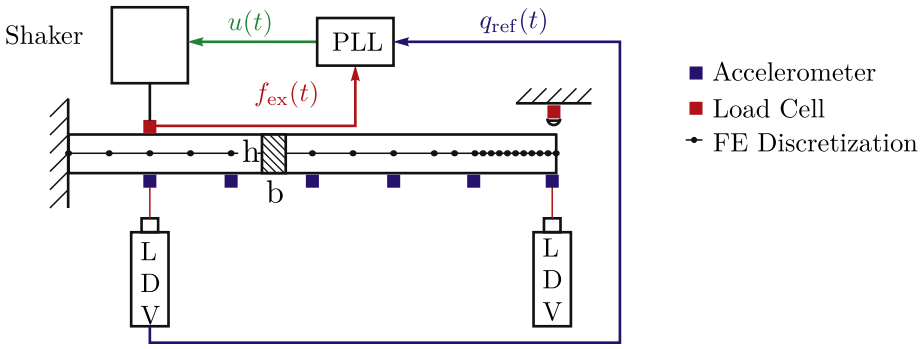

Fig. 6. Block diagram of PLL attached to a structure with shaker excitation.

Table 1
Linear eigenfrequencies and modal damping ratios of the first six bending modes of the beam (left) and parameters of the numerical beam models (right).

Frequency [Hz]	Damping [%]	Parameter	Value	Unit
40.10	0.19	E_{msh}	181.36	GPA
268.62	0.76	E_{hbm}	187.60	GPA
758.26	0.05	ρ	7730	kg/m^3
1371.82	0.17	h	20	mm
2427.72	0.10	b	12	mm
3508.31	0.14	$g_{0,i}$	1.03	mm

the density and the Young's modulus, the weight of the beam is used to calculate the density and the linear finite element model is updated subsequently such that the numerical eigenfrequencies match the measured eigenfrequencies. The obtained parameters are listed in Table 1 (right). Because the model with redistributed mass matrix is used for the MS-HBM, the model updating results in a slightly different parameter for the Young's modulus used for this method. To be more precise, the obtained parameter is slightly higher to compensate for the neglected mass of the contact node resulting in the same linear eigenfrequencies for the HBM and the MS-HBM model. Of course, the effect of the mass redistribution can also be compensated by changing the density parameter of the beam or by using more sophisticated optimization procedures. The linear model updating approach is used in this study for its effectiveness in the regarded example and its simplicity.

It is noted that in the experiment as well as in the numerical simulations the beam is regarded as one dimensional. Therefore, the local compression of the beam in the contact area is neglected which simplifies the analysis of the contact process.

5. Results and discussion

In this section, the experimental and numerical results obtained for the benchmark structure with the proposed methods are shown. In the first part, the impact process is analyzed in some detail and possible approaches for numerical modeling are discussed. In the second part of the section, the results of the experimental and numerical nonlinear modal analysis are presented and compared.

5.1. Characterization of the impact process

For the modeling of impact processes there exist numerous different methods [41]. Widespread methods to model restitution are the modeling with Newton's impact law or penalty methods, e.g., the modeling of the contact by a finite contact stiffness and damping parameter. Both methods have in common that they require design parameters which characterize the impact process. In the following the difficulties of identifying suitable parameters for such approaches is illustrated at the benchmark structure. Firstly, the identification of a coefficient of restitution for the modeling of dissipative behavior in Newton's law is addressed. Secondly, the identification of a finite contact stiffness parameter for modeling the elastic behavior of a penalty approach is discussed.

The use of a Newton impact law requires the choice of a coefficient of restitution

$$e_{\mathrm{N}} = -\frac{\gamma^{+}}{\gamma^{-}} \tag{29}$$

which describes the relation between the local post-impact velocity γ^{+} and pre-impact velocity γ^{-} at a contact DOF. Thereby, energy dissipation due to the impact can be modeled. In the benchmark experiment the pre- and post-impact velocity can be identified approximately by measuring the velocity at the beam tip at the time when the beam hits the stop $\gamma^{+} \approx \dot{q}_{\mathrm{tip}}(t_{\mathrm{con}})$

and separates from the stop $\gamma^- \approx \dot{q}_{\mathrm{tip}}(t_{\mathrm{sep}})$, respectively. The extracted coefficient of restitution is plotted over pre-impact velocity in Fig. 7 (a) along with the standard deviation for several impact processes. It can be observed that the coefficient of restitution depends on the pre-impact velocity in a non-trivial way. Furthermore, it can be seen that for higher pre-impact velocities the standard deviation increases. It has been observed during experimentation that this increase in the standard deviation is caused by local high frequency vibrations in the contact element. The experimental results illustrate that the identification of the parameter required for the use of a Newton impact law is difficult. The difficulties of identifying appropriate parameters along with the numerical issues described in Section 2.2 complicate the use of the conventional Newton impact law in the context of numerical nonlinear modal analysis.

An alternative modeling approach for the support element is the use of a finite contact stiffness model, i.e., replacing the stop by a linear spring (cf. Eq. (3)). To this end, an appropriate stiffness parameter has to be identified. In the benchmark experiment, the support element consists of a load cell, such that the contact force can be easily measured. Furthermore, the beam is modeled as one dimensional which facilitates the measurement of the position of the beam tip relative to the support element. The measured force over displacement is shown in Fig. 7 (b). Then, a linear function is fitted to the non-zero contact forces. The slope of the linear fit corresponds to the contact stiffness $k_{\mathrm{c}} = 2.3 \cdot 10^6$ N/m. This type of contact model can then be used for the calculation of the nonlinear modes with a conventional HBM approach.

The results show that the identification of design parameters for commonly used impact models is challenging, even for the relatively simple benchmark system. This is particularly the case for the Newton impact law which is, moreover, difficult to incorporate in a numerical nonlinear modal analysis method. The contact stiffness model can be used in this particular test case and is therefore used for comparison in the following. However, it is noted that the identification of the appropriate contact stiffness has only been possible here because the support element consists of a load cell and the beam has been modeled as one dimensional. In more general cases the measurement directly in the contact interface is infeasible.

5.2. Nonlinear numerical and experimental modal analysis

In this section, the results of the NEMA are shown and compared to numerical results obtained with the MS-HBM with massless boundary. Furthermore, the conventional HBM with a contact stiffness model is used for comparison. It is emphasized at this point that the results of the numerical nonlinear modal analysis are calculated independent of the NEMA results. For the MS-HBM only the linear model of the beam has been updated based on the results of the linear EMA. For the conventional HBM an updated linear model is used along with the contact stiffness identified as described above. For both numerical calculations the response is approximated with five harmonics. It has been observed that five harmonics are sufficient to accurately capture the global behavior of the system in this nonlinear mode in the energy range of interest. The choice of the number of considered harmonics is, particularly for nonsmooth systems, a nontrivial task. However, numerical studies with up to 20 harmonics have been carried out to verify that the effect of additional harmonics on the global dynamics is negligible. Moreover, the analysis of the experimental results suggests that the contributions of higher harmonics is comparatively small, also for the experimental setup, which is increasing the confidence of the choice made for the present example.

The nonlinear modal frequency over nonlinear modal amplitude is shown in Fig. 8 (a). The comparison of the numerical and experimental frequency-amplitude curves shows a very good agreement. It can be observed that the conventional HBM is slightly closer to the experimental curve compared to the MS-HBM. The MS-HBM seems to predict a stiffer contact behavior which can be attributed to the fact that the flexibility of the support element is neglected as it is modeled as unilateral constraint. It is expected that the accuracy can be increased by using a finite element model of the support element. In

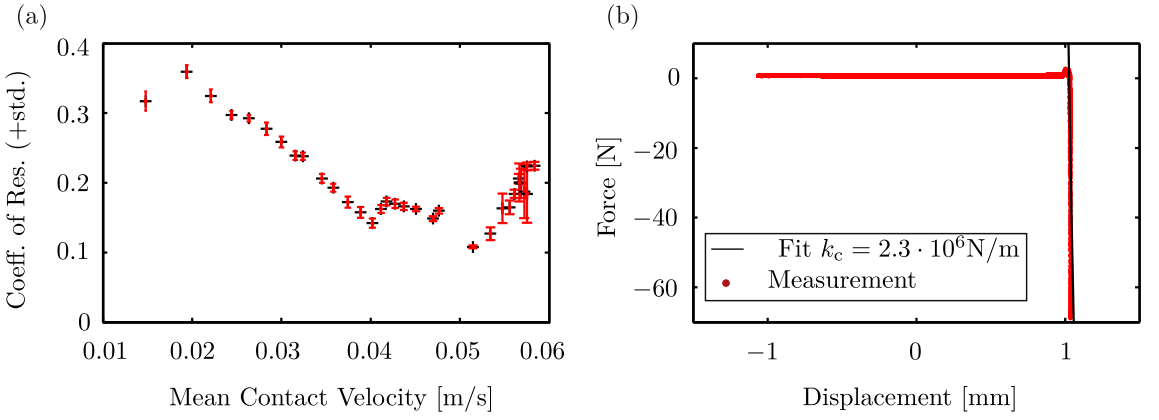

Fig. 7. Coefficient of restitution over pre-impact velocity with standard deviation (a) and measured contact force over displacement of the beam tip with linear fit (b).

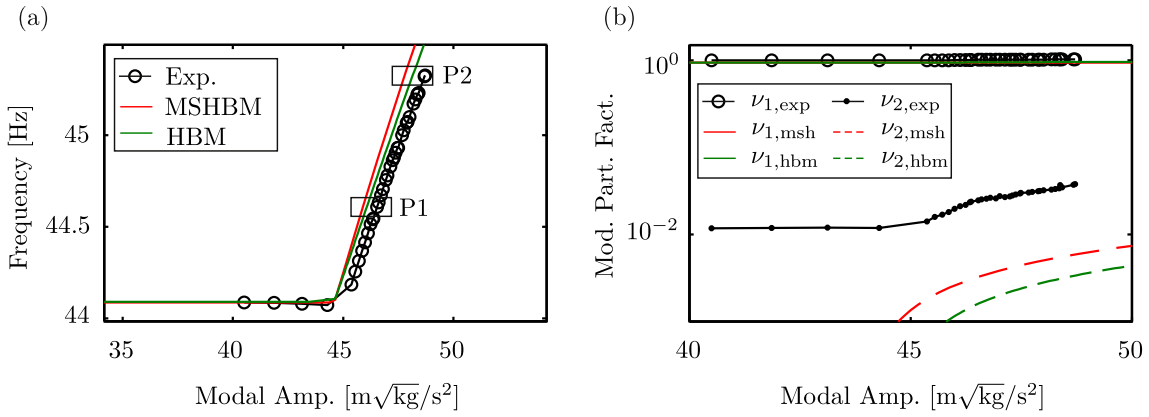

Fig. 8. Frequency-amplitude plot for experimental and numerical (MS-HBM and HBM) results of the first nonlinear mode (a) and modal participation factor of first and second linear modal coordinate (b).

contrast, the conventional HBM takes into account the flexibility of the contact element by the measured contact stiffness. It is emphasized, however, that the result of the conventional HBM generally depends on the contact stiffness. The identification of the appropriate parameter, which requires additional experimental effort, has only been possible in the special benchmark example, in which the contact force can explicitly measured. In more general cases this step requires considerable identification effort or the parameter is chosen in a heuristic way which reduces the confidence of the obtained results.

Next, the measured and simulated nonlinear mode shapes are analyzed. To this end, the nonlinear mode shape of the r-th mode is projected onto the linear modal space

$$\boldsymbol{v} = \sum_{n}^{N_h} \boldsymbol{\Phi}^{-1} \underline{\tilde{\boldsymbol{\phi}}}_{r,n}. \tag{30}$$

yielding the amplitude dependent participation factors of the linear modes. The results for the experiment and both numerical methods are shown in Fig. 8 (b) for the first two linear modal contributions. The contributions of the other modes were found to be negligible. It can be observed that for the experimental as well as both numerical results the contribution of the first linear mode dominates the motion. Indeed, the nonlinear modal motion is very similar to the first linear mode yielding a modal participation factor v_1 of approximately unity. This holds for the measured as well as the simulated results. The contribution of the second linear mode increases when the beam hits the stop but is about two orders of magnitude lower. For the numerical results the contribution of the second linear mode is (numerically) zero before the stop is reached as the linear eigenproblem is solved in this case. For graphical reasons, Fig. 8 (b), therefore, shows a zoom on the experimentally obtained curve. Generally, the contribution of the second linear mode is higher for the experimental results, even before the stop is reached, which may be attributed to experimental imperfections. However, the numerical results are qualitatively similar. Regarding the two different numerical methods, almost the same results are obtained. The predictions obtained with the MS-HBM seem to be slightly closer to experimental reality in this respect.

The motion of the beam tip is analyzed in more detail in the time domain in Fig. 9 for the two reference points marked on the frequency-amplitude plot shown in Fig. 8 (a). The time signal for the displacement and the contact force for P1 are shown in Fig. 9 (a) and (b). Herein, the blue line marks the distance to the stop element and the red circle the point when the beam hits the stop and the green circle the point when the beam separates from the stop. It can be seen that the displacement signal of the experiment and both numerical methods agree almost perfectly. In the time signal of the contact force, however, differences become apparent. The MS-HBM qualitatively captures the behavior of the measured force but the maximum value is overpredicted which corresponds to the too stiff contact behavior that has also been observed in the frequency-amplitude curve. For the conventional HBM a significant smearing of the peak and underestimation of the maximum value can be observed, which is caused by the comparatively rough approximation with five harmonics. It is interesting to note, however, that the effect on the displacement response seems to be negligible. For the displacements and contact forces at P2 in Fig. 9 (c) and (d) similar results are obtained. In the measured contact force for P2 it can be seen that a small side-peak appears next to the primary peak which cannot be predicted by the numerical simulations. This small peak is caused by local high frequency dynamics in the contact interface which cannot be captured by the approximate solution with five harmonics and the comparatively coarse discretization of the beam. It has been observed during experimentation that the high frequency vibrations do not correspond to the bending modes of the beam, but are caused by local flexibility of the beam and the load cell located in the stop element. In particular, local high frequency vibrations have been observed in the load cell which are likely to cause the measured side peak. To capture such local effects numerically, a much more detailed model of the system including the stop element would be necessary.

It is found quite remarkable that the measured displacement signal at the beam tip seems to be almost sinusoidal although the structure is subjected to the severe nonsmooth impact nonlinearity. Obviously, this is also the reason why a

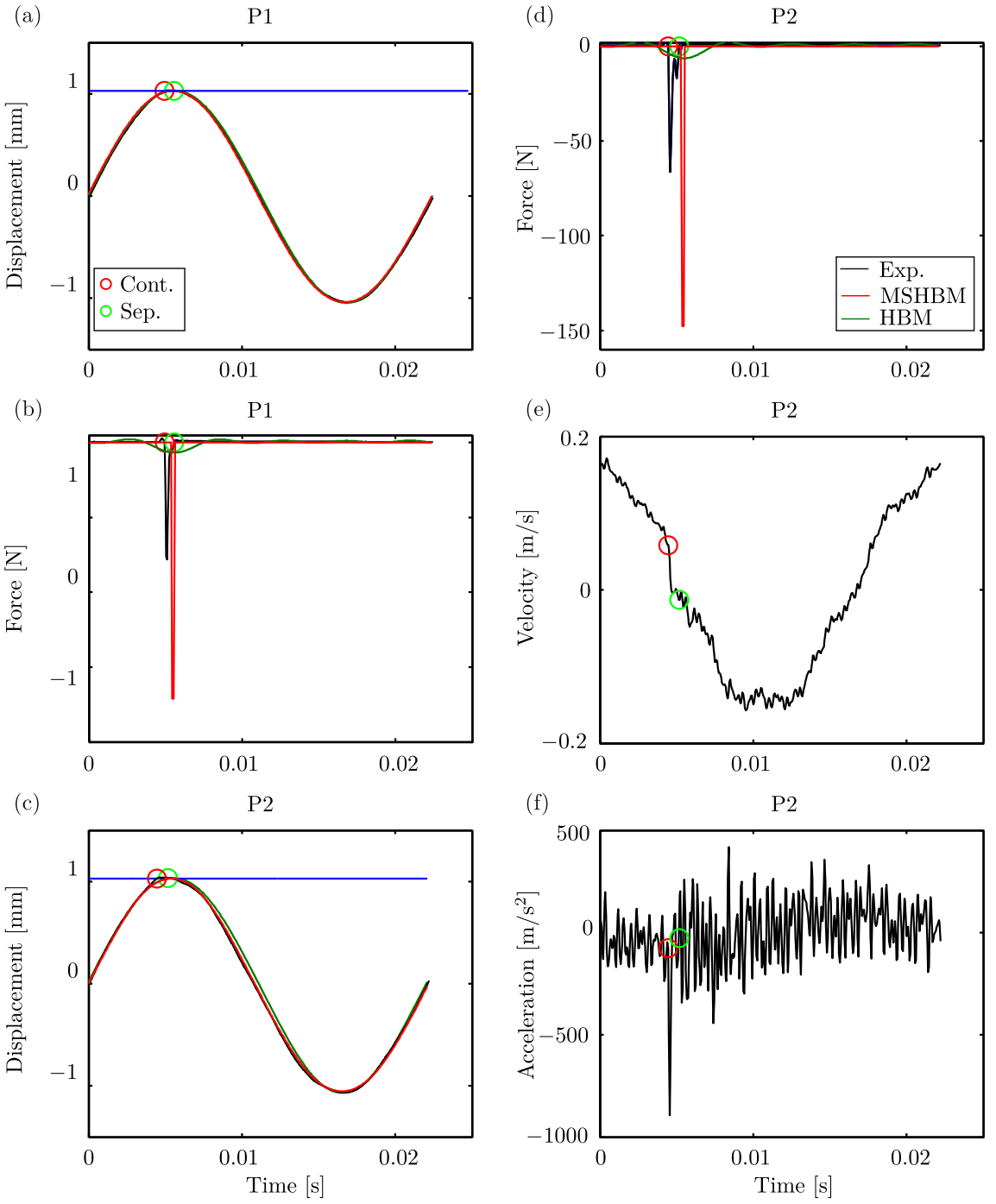

Fig. 9. Time histories for the displacement (a) and contact force (b) for P1 and time histories for displacement (c), contact force (d), velocity (e) and acceleration (f) for P2.

good numerical result with the MS-HBM and the HBM can be obtained with only five harmonics. In contrast, the measured velocity and acceleration signal for P2 shown in Fig. 9 (e) and (f) show significant high frequency content. These high frequency vibrations, however, do not seem to have a strong influence on the global behavior of the structure.

The measured nonlinear modal damping characteristic is shown in Fig. 10 (a). The damping behavior cannot be compared to numerical data because the numerical calculations are made based on the conservative autonomous system. The damping measure which is calculated based on the active power of the excitation forces shows linear behavior before the beam hits the stop. When the beam hits the stop the effective damping increases. This increase in damping may be caused by the power

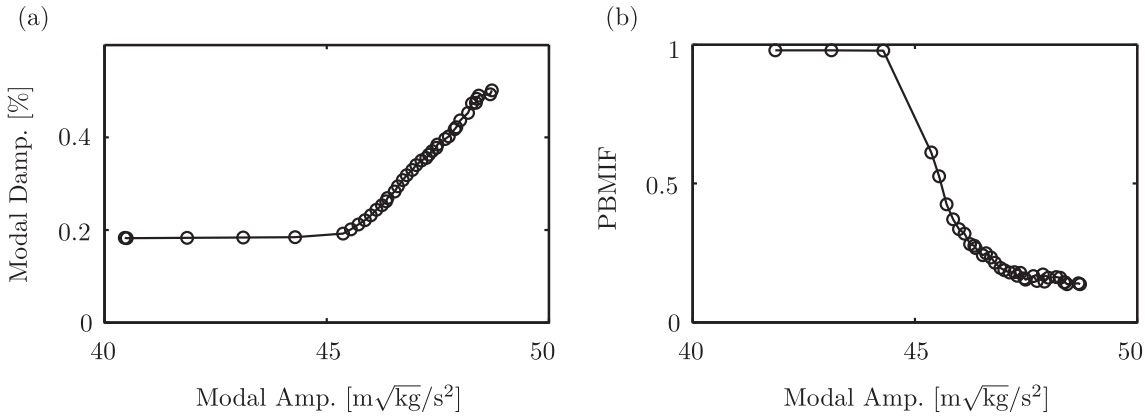

Fig. 10. Experimentally extracted amplitude dependent damping (a) and PBMIF (b).

transfer to high frequencies (cf. Fig. 9 (e) and (f)) due to the impact, where the vibration energy is then attenuated. Furthermore, friction in the contact interface may play a role.

Finally, the mode isolation quality is evaluated based on the PBMIF in Fig. 10 (b). It can be seen that the mode isolation quality significantly decreases when the impact is reached. This indicates that the single point single harmonic force may not be sufficient for an exact mode isolation. It has been observed during experimentation that particularly high harmonic distortions in the force and velocity signal are the reason for the decrease. Therefore, the control of additional frequencies may increase the mode isolation quality. Despite these discrepancies, the comparison of the frequency and shape of the simulated nonlinear modes (cf. Fig. 8) shows a very good agreement.

6. Conclusion and future work

This paper proposes a novel method for the numerical and experimental nonlinear modal analysis of nonsmooth mechanical systems. The numerical method is based on a mixed time-frequency domain representation of a system modeled by finite elements with a massless boundary. The massless boundary approach allows for the transformation of dynamic contact problems into a quasi-static contact problem which can be solved without the need for any contact parameters or impact law. Furthermore, the method provides energy conservation and the possibility of filtering internal resonances which can considerably reduce the computational burden compared to conventional time-domain approaches. The experimental method is based on a rigorous extension of nonlinear phase resonance testing, which has hitherto only been applied to smooth nonlinear systems, to nonsmooth structures. The PLL based approach is highly robust and can easily be automated.

A benchmark beam structure is used to illustrate the numerical and experimental approach. The good agreement of the numerically and experimentally obtained nonlinear modal parameters proves the applicability of the methods. It is found particularly remarkable in this context that the numerical model has been obtained without the need for any nonlinear system identification.

Further steps involve the inclusion of damping models in the numerical simulations. The use of the extended periodic motion concept for nonconservative systems may provide an interesting path forward in this respect [16,42]. An additional open research question is the increase of the mode isolation quality, e.g., by the control of higher harmonic frequencies, to further increase the quality of the measurements. Moreover, the study of more complex structures with a stronger change in the nonlinear mode shape will be investigated.

References

[1] M. Krack, L. Salles, F. Thouverez, Vibration prediction of bladed disks coupled by friction joints, Arch. Comput. Methods Eng. 24 (3) (2017) 589–636.
[2] A.F. Vakakis, O.V. Gendelman, L.A. Bergman, D.M. McFarland, G. Kerschen, Y.S. Lee, Nonlinear Targeted Energy Transfer in Mechanical and Structural Systems, vol. 156, Springer Science & Business Media, 2008.
[3] O.V. Gendelman, A. Alloni, Dynamics of forced system with vibro-impact energy sink, J. Sound Vib. 358 (2015) 301–314.
[4] M.A. AL-Shudeifat, A.F. Vakakis, L.A. Bergman, Shock mitigation by means of low- to high-frequency nonlinear targeted energy transfers in a large-scale structure, J. Comput. Nonlinear Dyn. 11 (2) (2015) 1–11.
[5] R.M. Rosenberg, Normal modes of nonlinear dual-mode systems, J. Appl. Mech. 27 (2) (1960) 263–268.
[6] G. Kerschen, M. Peeters, J.C. Golinval, A.F. Vakakis, "Nonlinear normal modes, part I: A useful framework for the structural dynamicist, Mech. Syst. Signal Processing 23 (1) (2009) 170–194.
[7] Y.V. Mikhlin, K.V. Avramov, Nonlinear normal modes for vibrating mechanical systems. Review of theoretical developments, Appl. Mech. Rev. 63 (6) (2010) 060802-1–060802-21.
[8] K.V. Avramov, Y.V. Mikhlin, Review of applications of nonlinear normal modes for vibrating mechanical systems, Appl. Mech. Rev. 65 (2) (2013) 020801-1–020801-20.
[9] M. Peeters, R. Viguié, G. Sérandour, G. Kerschen, J.C. Golinval, Nonlinear normal modes, part II: toward a practical computation using numerical continuation techniques, Mech. Syst. Signal Processing 23 (1) (2009) 195–216.

[10] R. Arquier, S. Bellizzi, R. Bouc, B. Cochelin, Two methods for the computation of nonlinear modes of vibrating systems at large amplitudes, Comput. Struct. 84 (24) (2006) 1565–1576.
[11] S. Peter, R.I. Leine, "Excitation power quantities in phase resonance testing of nonlinear systems with phase-locked-loop excitation, Mech. Syst. Signal Processing 96 (2017) 139–158.
[12] M. Peeters, G. Kerschen, J.C. Golinval, Dynamic testing of nonlinear vibrating structures using nonlinear normal modes, J. Sound Vib. 330 (3) (2011) 486–509.
[13] D.A. Ehrhardt, M.S. Allen, Measurement of nonlinear normal modes using multi-harmonic stepped force appropriation and free decay, Mech. Syst. Signal Processing 76–77 (2016) 612–633.
[14] C.H. Lamarque, O.V. Gendelman, A. Ture Savadkoohi, E. Etcheverria, Targeted energy transfer in mechanical systems by means of non-smooth nonlinear energy sink, Acta Mech. 221 (1–2) (2011) 175–200.
[15] D. Laxalde, F. Thouverez, Complex non-linear modal analysis for mechanical systems: application to turbomachinery bladings with friction interfaces, J. Sound Vib. 322 (2009) 1009–1025.
[16] M. Krack, Nonlinear modal analysis of nonconservative systems: extension of the periodic motion concept, Comput. Struct. 154 (2015) 59–71.
[17] R.I. Leine, H. Nijmeijer, Dynamics and Bifurcations of Non-Smooth Mechanical Systems, vol. 18, Springer-Verlag, Berlin Heidelberg New-York, 2004.
[18] Y.S. Lee, F. Nucera, A.F. Vakakis, D.M. McFarland, L.A. Bergman, Periodic orbits, damped transitions and targeted energy transfers in oscillators with vibro-impact attachments, Physica D 238 (18) (2009) 1868–1896.
[19] T. Detroux, L. Renson, and G. Kerschen, The Harmonic Balance Method for advanced analysis and design of nonlinear mechanical systems, in: Proceedings of the SEM IMAC XXXII, 2014.
[20] E.P. Petrov, D.J. Ewins, Analytical formulation of friction interface elements for analysis of nonlinear multi-harmonic vibrations of bladed discs, Proc. ASME Turbo Expo (2002).
[21] S. Nacivet, C. Pierre, F. Thouverez, L. Jezequel, A dynamic Lagrangian frequency-time method for the vibration of dry-friction-damped systems, J. Sound Vib. 265 (1) (2003) 201–219.
[22] F. Schreyer, R.I. Leine, A mixed shooting-harmonic balance method for unilaterally constrained mechanical systems, Arch. Mech. Eng. 63 (2) (2016) 297–314.
[23] J.M. Londono, S.A. Neild, J.E. Cooper, Identification of backbone curves of nonlinear systems from resonance decay responses, J. Sound Vib. 348 (2015) 224–238.
[24] M. Peeters, G. Kerschen, J.C. Golinval, Modal testing using nonlinear normal modes: an experimental demonstration, in: Proceedings of ISMA, (Leuven), pp. 3221–3236, 2010.
[25] L. Renson, A. Gonzalez-Buelga, D. Barton, S. Neild, Robust identification of backbone curves using control-based continuation, J. Sound Vib. 367 (2016) 145–158.
[26] V. Denis, M. Jossic, C. Giraud-Audine, B. Chomette, A. Renault, O. Thomas, Identification of nonlinear modes using phase-locked-loop experimental continuation and normal form, Mech. Syst. Signal Processing 106 (2018) 430–452.
[27] N. Huang, H. Shih, C. Tung, S. Long, N. Yen, Q. Zheng, M. Wu, Z. Shen, H. Liu, The empirical mode decomposition and the Hilbert spectrum for nonlinear and non-stationary time series analysis, Proc. R. Soc. A: Math., Phys. Eng. Sci. 454 (1971) (1998), pp. 995, 903.
[28] Y.S. Lee, A.F. Vakakis, D.M. McFarland, L.A. Bergman, Non-linear system identification of the dynamics of aeroelastic instability suppression based on targeted energy transfers, Aeronaut. J. 114 (1152) (2010) 61–82.
[29] M. Eriten, M. Kurt, G. Luo, D.M. McFarland, L.A. Bergman, A.F. Vakakis, Nonlinear system identification of frictional effects in a beam with a bolted joint connection, Mech. Syst. Signal Processing 39 (1) (2013) 245–264.
[30] S. Peter, R. Riethmüller, R.I. Leine, Tracking of backbone curves of nonlinear systems using phase-locked-loops, in: G. Kerschen (Ed.), Nonlinear Dynamics, Volume 1, Proceedings of the 34th IMAC, A Conference and Exposition on Structural Dynamics, 2016, pp. 107–120, ch. 11.
[31] S.W. Shaw, C. Pierre, Normal modes for non-linear vibratory systems, J. Sound Vib. 164 (1) (1992) 85–124.
[32] F. Schreyer, R.I. Leine, Mixed Shooting-HBM: A periodic solution solver for unilaterally constrained systems, in: Proceedings of IMSD, (Montreal), 2016.
[33] H.B. Khenous, P. Laborde, Y. Renard, Mass redistribution method for finite element contact problems in elastodynamics, Eur. J. Mech., A/Solids 27 (5) (2008) 918–932.
[34] M. Krack, L. Panning-von Scheidt, J. Wallaschek, A method for nonlinear modal analysis and synthesis: application to harmonically forced and self-excited mechanical systems,", J. Sound Vib. 332 (25) (2013) 6798–6814.
[35] A. Dhooge, W. Govaerts, Y.A. Kuznetsov, MATCONT: a MATLAB package for numerical bifurcation analysis of ODEs, ACM Trans. Math. Softw. 29 (2) (2003) 141–164.
[36] J.L. Zapico-Valle, M. García-Diéguez, R. Alonso-Camblor, Nonlinear modal identification of a steel frame, Eng. Struct. 56 (2013) 246–259.
[37] S. Peter, M. Scheel, M. Krack, R.I. Leine, Synthesis of nonlinear frequency responses with experimentally extracted nonlinear modes, Mech. Syst. Signal Processing 101 (2018) 498–515.
[38] I. Sokolov, V. Babitsky, Phase control of self-sustained vibration, J. Sound Vib. 248 (4) (2001) 725–744.
[39] V.I. Babitsky, I.J. Sokolov, Autoresonant homeostat concept for engineering application of nonlinear vibration modes, Nonlinear Dyn. 50 (3) (2007) 447–460.
[40] D.J. Ewins, Modal testing: Theory, Practice and Application, 2. ed., Baldock: Research Studies Press Ltd, 2000.
[41] R.A. Ibrahim, Vibro-impact Dynamics: Modeling, Mapping and Applications, vol, Springer Science & Business Media, 2009, p. 43.
[42] M. Scheel, S. Peter, R.I. Leine, M. Krack, A phase resonance approach for modal testing of structures with nonlinear dissipation, J. Sound Vib. 435 (2018) 56–73.